CHAPTER 1

Introduction

A major challenge for an inter-disciplinary program such as neuroscience is the integration of ideas within the disciplines to achieve a common goal. Apart from doing research in respective disciplines and catering to their audience, neuroscience as an inter-disciplinary field must cross the hurdle of discipline unification to achieve any significant strides in understanding the complexities of human brain. In other words, neuroscientists in their respective disciplines must build their research, and hence understanding, upon researches of their colleagues from other disciplines. This thesis is an essay on a quantitative method of disciplinary model integration.

If we consider respective disciplines as rungs of a ladder (Fig. 1.1), the objective of a neuroscientist should be to join the rungs for achieving the common goal of understanding how brain works. Taking the concept from systems theory this can be done on two accounts: model-order reduction (MOR) and scientific reduction (SR). MOR is the simplification of the amount of detail needed in obtaining computationally tractable models of ever more complex systems. Thus with MOR one moves towards increasing level of abstraction from mechanism to behavior. SR on the other hand is migrating scientific study and theory from the level of phenomena more directly observable by our senses to levels of increasingly refined scientific constructs.

This thesis deals with the particular problem of designing a pulse-coded neural network (PCNN) and achieving an adaptive PCNN (APCNN) based on brain function. It will be shown that this problem can be tackled by implementing the model-reference

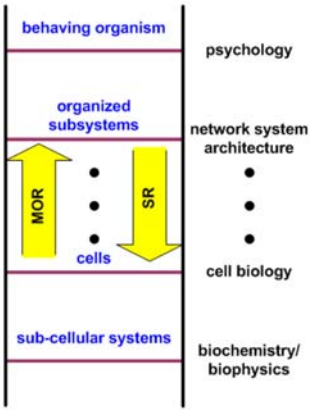

Figure 1.1. Neuroscience ladder adopted from [Wells 2011a] showing several rungs each representing scientific construct at various levels. Moving upward towards increasing level of abstraction from mechanism to behavior is model-order reduction (MOR). However, migration of scientific study from level of observable phenomenon down to increasingly refined scientific constructs is scientific reduction (SR).

principle from systems theory [Widrow & Sterns 1985]. The reference model is a network designed by Grossberg [Grossberg 1972b] which is based on psychological principles, hence described by activity level, and thus a level-coded model. This level-coded model is taken as the reference model because of its adaptive ability. A PCNN is then designed based upon the Eckhorn neuron model [Eckhorn et al. 1989b, 1990] such that it exhibits properties corresponding to those of the pre-adapted level-coded model. Finally, performance of the PCNN is evaluated against the level-coded model to achieve the adaptive property of the level-coded model, hence achieving an APCNN.

The level-coded model representing psychological phenomenon is situated close to the psychological rung while the pulse-coded model is relatively closer to the biological/physiological rung (Fig. 1.2). Therefore, the approach in this thesis is SR as we implement level-coded model in order to incorporate its properties into a model with significantly more parts, the pulse-coded model.

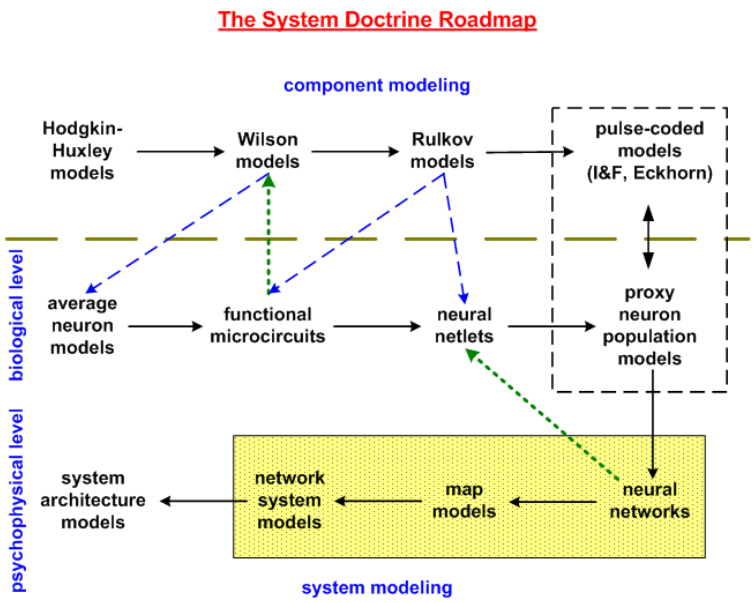

Figure 1.2. An alternate view of the neuroscience ladder (Fig. 1.1), neuroscience roadmap. The highlighted region indicates the location of this thesis with regards to the neuroscience roadmap. Thus, the level-coded model based on psychological principles is close to the psychophysical end while the pulse-coded model built using Eckhorn neuron model is relatively closer to the physiological end of the roadmap. A map model is a network of neural networks while a network of maps comprises a network system [Wells 2010, Ch.7].

Grossberg's Network

Grossberg's network (G-N) is based on psychological postulates made by Grossberg [Grossberg 1972a] which can be summarized as follows. When a subject receives shock (unconditioned stimulus) that induces fear, the subject experiences relief from fear of the shock immediately after the removal of shock stimulus. These fear and relief responses form what Grossberg calls the net-incentive motivation. In addition, the generation of fear or relief response can be reinforced by another external stimulus (conditioning stimulus). This learning of motivation patterns forms the reinforcement.

The network model derived from the above postulates has three representations: sensory, drive and motor representations (Fig. 1.3). The sensory representation sending

conditioning stimulus reinforces the drive representation. The drive representation formed by a dipole network (DN) generates motivational decisions in psychological terms. And finally, the motor representation receiving inputs from the other two representations generates action (motor) commands. The dipole network plays an important role in supporting the postulates. The unique property of the dipole network constructed by Grossberg is the rebound mechanism. That is, relief response occurs when shock input (for fear) is removed.

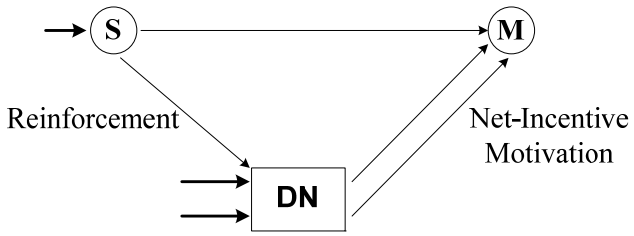

Figure 1.3. The three representations for deriving the Grossberg network; S, sensory representation receiving conditioning stimulus; DN, drive representation receiving tonic and unconditioned stimulus; and M, motor representation receiving inputs from the former two. The dipole network (DN) forms the drive representation and plays an important role in supporting Grossberg's psychological postulates. In psychological terms, outputs from DN correspond to net-incentive motivation and outputs from S to DN correspond to reinforcement. Finally, action or motor commands are generated by M.

The law of the dipole network deduced by Grossberg [Grossberg 1969a, 1969b, 1971] is expressed as

$$\dot{x}_i = -\varepsilon_i \cdot x_i + \sum_{k=1}^{n} \zeta_{ki} \cdot [x_k(t - \tau_{ki}) - \Gamma_{ki}]^+ \cdot z_{ki} + I_i, \qquad (1)$$

$$\dot{z}_{jk} = \beta_{jk} \cdot (\gamma_{jk} - z_{jk}) - \delta_{jk} \cdot [x_j(t - \tau_{jk}) - \Gamma_{jk}]^+ \cdot z_{jk} \qquad (2)$$

where $x_i(t)$ = activity of i^{th} node within the network, I_i = stimulus to i^{th} node, ζ is an excitation rate, δ is the adaptation rate, Γ denotes threshold, ε and β are the relaxation

rates, and $z_{ki}(t)$ = elastic connection strength (memory trace) from k^{th} to i^{th} node. γ is the maximum connection strength and τ is the adaptation lag. The Heaviside extractor activation function $[H]^+$ is given by, $[H]^+ = \begin{cases} H, \text{ if } H > 0 \\ 0, \text{ if } H \le 0. \end{cases}$

The law therefore describes the interaction of node activity with connection strength (synaptic weight). The external event via input I_i excites node activity $x_i(t)$ increased by an amount determined by the second term of equation (1), which is the sum of the products of preceding node activities with respective synaptic weight. The decrease in $x_i(t)$ node activity is proportional to its initial activity, given by the first term. For τ_{ki} = 0, the steady-state solution of i^{th} node activity is

if $x_i > \Gamma_{ii}$,

$$x_i = \frac{I_i - \zeta_{ii} \cdot \Gamma_{ii} \cdot z_{ii} + \sum_{k=1,k\neq i}^{n} \zeta_{ki} \cdot [x_k(t) - \Gamma_{ki}]^+ \cdot z_{ki}}{\varepsilon_i - \zeta_{ii} \cdot z_{ii}} > \Gamma_{ii}$$

else if $x_i \le \Gamma_{ii}$,

$$x_i = \frac{I_i + \sum_{k=1,k\neq i}^{n} \zeta_{ki} \cdot [x_k(t) - \Gamma_{ki}]^+ \cdot z_{ki}}{\varepsilon_i} \le \Gamma_{ii}.$$

Equation (2) on the other hand describes the rate of elastic synaptic weight formation. The steady-state weight is

$$z_{jk} = \frac{\beta_{jk} \cdot \gamma_{jk}}{\beta_{jk} + \delta_{jk} \cdot [x_j(t - \tau_{jk}) - \Gamma_{jk}]^+} \le \gamma_{jk}.$$

Note that for $\delta_{jk} = 0$, $z_{jk} = \gamma_{jk}$, a fixed value.

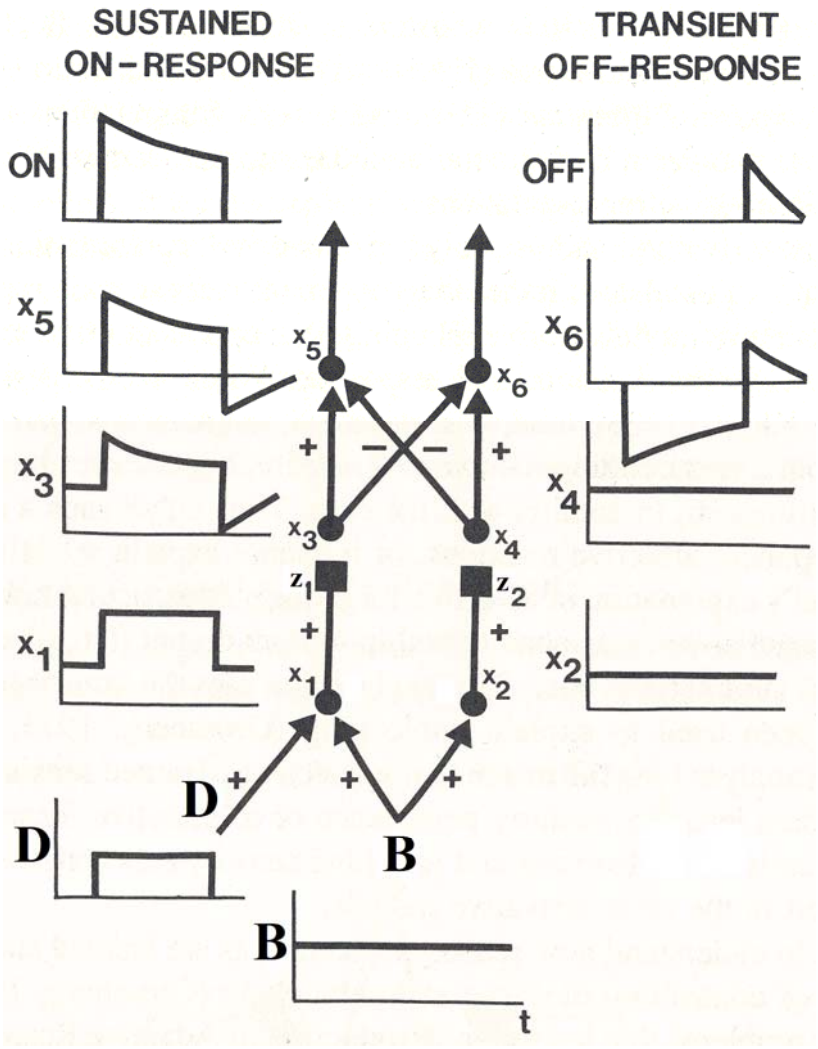

Figure 1.4. Dipole Network (DN) derived by Grossberg using equations (3) to (12) receiving bias or tonic input (B) and drive or shock input (D). x_1 and x_2 represent node activities at first stage of processing in response to respective input stimulus. x_3 and x_4 activities at second stage respond to the preceding node activities (x_1 & x_2) connected by respective elastic weights (z_1 & z_2). Input for generating x_5 and x_6 activities at third stage is the result of mutual inhibition between x_3 and x_4 activities. DN outputs are the result of x_5 and x_6 activities. The plots at the side of the network represent the node activities at respective stage of processing derived analytically with the exception of bottom and top two, which are DN inputs and outputs respectively adopted from [Grossberg et al. 1991]. $x_i < 0$ denotes below-normal-background activity.

Grossberg [Grossberg 1972b] used the principles of above two equations (Eqn. 1 & 2) to design the dipole network shown in Figure 1.4. The process describing the network is given by

$$\dot{x}_1 = -\alpha \cdot x_1 + B + D, \tag{3}$$

$$\dot{x}_2 = -\alpha \cdot x_2 + B, \tag{4}$$

$$\dot{z}_1 = \beta \cdot (\gamma - z_1) - \delta \cdot [x_1(t-\tau) - \Gamma]^+ \cdot z_1, \tag{5}$$

$$\dot{z}_2 = \beta \cdot (\gamma - z_2) - \delta \cdot [x_2(t-\tau) - \Gamma]^+ \cdot z_2, \tag{6}$$

$$\dot{x}_3 = -\varepsilon \cdot x_3 + \zeta \cdot [x_1(t-\tau) - \Gamma]^+ \cdot z_1, \tag{7}$$

$$\dot{x}_4 = -\varepsilon \cdot x_4 + \zeta \cdot [x_2(t-\tau) - \Gamma]^+ \cdot z_2, \tag{8}$$

$$\dot{x}_5 = -\omega \cdot x_5 + \kappa \cdot [x_3(t-\sigma) - x_4(t-\sigma)]^+, \tag{9}$$

$$\dot{x}_6 = -\omega \cdot x_6 + \kappa \cdot [x_4(t-\sigma) - x_3(t-\sigma)]^+, \tag{10}$$

$$O_5 = \lambda \cdot [x_5 - \Omega]^+, \tag{11}$$

$$O_6 = \lambda \cdot [x_6 - \Omega]^+. \tag{12}$$

Equations (3) and (4) describes the node activities at first stage of input processing, whose response is linear to their inputs, bias (B) or tonic input and drive (D) or shock input, and bias (B) input alone respectively. Equations (7) and (8) describe node activities at the second stage of processing connected to the first stage nodes via elastic weights, given by (5) and (6) respectively. The weight formation follows the law described earlier. Node activity (Eqn. 9 & 10) at the third stage of processing receives competitive signal inputs generated by the preceding node activities. In other words, node-3 and node-4 outputs are processed by a subtractive on-off field yielding inputs to node-5 and node-6. Finally, output of the DN is given by equations (11) and (12) which are activation functions of respective third stage node activities.

The properties of the network leading to the rebound mechanism as described by Grossberg [Grossberg 1972b] can be summarized as follows:

- Termination of drive input unmasks the effects of an internally driven input to cause transient off-response (output from x_6 activity). This internal source is the level (γ) sought by the weight formation (z_2, Eqn. 6) when there is no preceding node activity. Hence this internal source or level is neither turned on nor off by the drive input.

- Internal source or level accumulates (summates) when drive input is on. That is, drive input summates with bias input.

- The transient off-response (O_6) shuts off soon after it is turned on because with just bias input, the equivalent x_3 and x_4 activity levels competing by mutual inhibition results in no input for nodes at third stage of the processing. Thus, there is no x_5 and x_6 activity.

The original dipole network by Grossberg did not present a long-term adaptive function. However, this thesis implements Grossberg's network with long-term adaptive capability. The adaptation occurs at the weights connecting the sensory inputs (from sensory representation, Fig. 1.3) to the dipole network. Adaptation of these weights is based on Grossberg's outstar rule [Grossberg 1978]. In psychological terms, adaption of the network implies that the conditioning (sensory) stimulus, by association with unconditioned (drive) stimulus, leads to a conditioned response for activities from the motor representation. A detailed qualitative and quantitative description of the adaptive capability of the network is given in the next chapter.

Eckhorn Neuron Model

Eckhorn and coworkers demonstrated in cat primary visual cortex that stimulus-evoked oscillations of local processing units representing local visual features get transiently locked into a common resonance state by appropriate global stimulus [Eckhorn et al. 1988a, 1988b, 1989a]. Activities of these neural groups become synchronized, representing feature linking via visual stimulus. The Eckhorn neuron model is the product of Eckhorn's et al. [Eckhorn et al. 1989b] search for physiological explanation (mechanism) of transient linking of local visual features into global coherent percepts. Based on the neuro-physiological findings, they designed a neural network model capable of performing feature linking via modulatory interactions. This neural network consisted of two one-dimensional layers of proxy neuron population models. We shall call these models Eckhorn Neural Units (ENUs) [Wells 2010, Ch8].

The ENU has two main parts. The first part receives external inputs and the second receives inputs from the first (Fig. 1.5). These components are named dendrite and soma, respectively. However, one should be warned that these two terms are not to be confused with the dendrites and soma of a biological neuron. The dendrite compartment can further be sub-divided with respect to the two functionally different inputs for soma it generates. These are the regular "feeding" inputs and modulatory "linking" inputs. Eckhorn et al. uses the term modulatory (as in amplitude modulation of a radio-frequency carrier) for linking signals due to its modulatory effect on the feeding signals. Within their network, the concept of the linking field was introduced as a correspondence to the association field of a local assembly of visual neurons providing the linking mechanism in perceptual feature linking [Eckhorn et al. 1990].

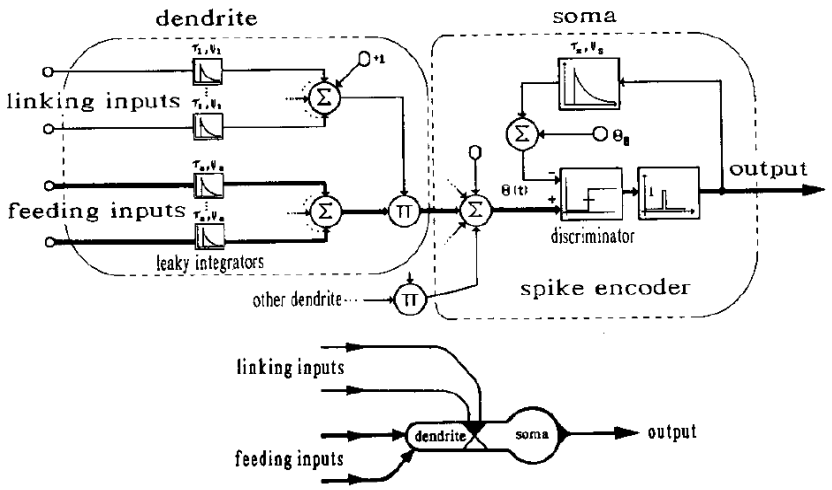

Figure 1.5. Basic Eckhorn neural unit (ENU) having two components (dendrite & soma). Inset shows internal workings in the components (adopted from [Eckhorn et al. 1990]).

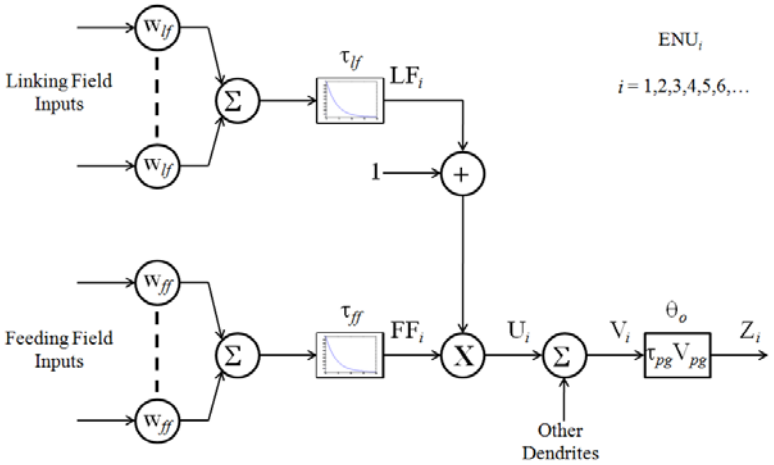

Figure 1.6. Another view of the above basic ENU architecture. Subscript of ENU$_i$ is such that i denotes one specific ENU. The feeding field input value is either 0 or 1.
Linking field: w_{lf} & τ_{lf} are parameters (weight & time constant) and LF_i the output.
Feeding field: w_{ff} & τ_{lf} are parameters (weight & time constant) and FF_i the output.
Soma/Neuromime Pulse Generator (NMPG): τ_{pg}, V_{pg} & θ_o (time constant, threshold amplitude & threshold offset) and Z_i (spike output).

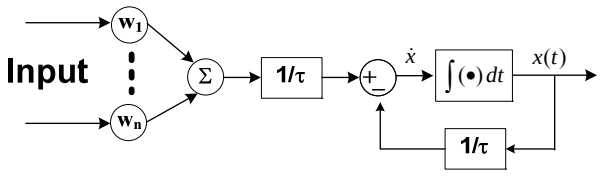

Figure 1.7. Block diagram of the leaky-integrator (LI). Feed-forward gain ($1/\tau$) is used to make the transfer function have unity gain for step function inputs. This implementation is shown in equations (13) and (14).

For a detailed description of the ENU one must consider the quantitative relationship within and between the components. Figure 1.6 shows a detailed representation of figure 1.5. The difference equations for the mathematical description [Eckhorn et al. 1990] are

$$FF_i(t) = FF_i(t-\Delta t)\cdot\exp(-\Delta t/\tau_{ff}) + (1/\tau_{ff})\cdot w_{ff}\cdot\sum_{\forall j} F_j^{inputs}, \quad (13)$$

$$LF_i(t) = LF_i(t-\Delta t)\cdot\exp(-\Delta t/\tau_{lf}) + (1/\tau_{lf})\cdot w_{lf}\cdot\sum_{\forall j} L_j^{inputs}, \quad (14)$$

$$U_i(t) = FF_i(t)\cdot(1 + LF_i(t)), \quad (15)$$

$$V_i(t) = \sum_{\forall i} U_i(t), \quad (16)$$

$$\Theta_{V_i}(t+\Delta t) = \begin{cases} V_{pg}, & V_i(t) \geq \Theta_i(t) \\ \Theta_{V_i}(t)\cdot\exp(-\Delta t/\tau_{pg}), & V_i(t) < \Theta_i(t) \end{cases}, \quad (17)$$

$$\Theta_i(t) = \Theta_O + \Theta_{V_i}(t), \quad (18)$$

$$Z_i(t+\Delta t) = \begin{cases} 1, & V_i(t) \geq \Theta_i(t) \\ 0, & V_i(t) < \Theta_i(t) \end{cases}. \quad (19)$$

The feeding and linking inputs for the soma are generated by their respective leaky-integrator functions (Eqn. 13 & 14). The leaky-integrators integrate the weighted afferent signals at respective rates given by their time constants, τ_{ff} and τ_{lf} . These integrated signals then leak exponentially at their rates. Eckhorn et al. used a time-step (Δt) of 1ms for their simulations [Eckhorn et al. 1990]. The LFLI together with a constant offset term (+1) interacts multiplicatively with the FFLI resulting in amplitude modulation of the FFLI output (Eqn. 15). Thus, the two parts of the dendrite components come together to form the dendrite output (U_i).

Depending upon the presence of other dendrite components, the respective dendrite outputs are summed to form the soma input (V_i) signal (Eqn. 16). The soma component as a neuromime is represented by the two-state variables (Θ_{V_i} & Z_i) to generate pulses from i^{th} ENU (Eqns. 17, 18, 19). Thus, equation (19) shows that if $V_i <$ neuromime threshold (Θ_i), there is no output from the soma. However if $V_i \geq \Theta_i$, the output is 1, resulting in pulse generation. In addition equation (17) shows that the $V_i \geq \Theta_i$ condition also resets the neuromime threshold ($\Theta_i = V_{pg}$) corresponding to an absolute refractory period. This is followed by an exponential decay at a rate given by the time constant τ_{pg} when soma input returns to the $V_i < \Theta_i$ case. This exponential decay of Θ_i to its resting level (Θ_O) corresponds to a relative refractory period.

Pulse-mode firing resulting from the above mechanisms can be classified into types: all-pass mode, high-pass mode, rate-multiplier mode and saturated mode (Fig. 1.8). The saturated mode is an original finding in this thesis. During all-pass firing mode (Fig. 1.8a), every input stimulus produces soma input exceeding the neuromime threshold, i.e., $V_i \geq \Theta_i$. All-pass mode occurs if the condition, $\frac{V_{ff}}{\tau_{ff}} \geq \Theta_o$ is satisfied ($V_{ff} = \sum_{\forall j} w_{ff_j} \cdot F_j^{inputs}$).

In high-pass mode (Fig. 1.8b), ENU spiking occurs such that the interval of the successful inputs are wider than the actual inter-input interval (Fig. 1.9). That is, ENU in this mode perform as a high-pass like filter as they filter out lower frequency inputs. For a long input tetanus at spike interval T, the FFLI output has a DC base, $\frac{1}{\mathrm{T}} \sum_{\forall j} w_{ff_j} \cdot F_j^{inputs}$.

Thus with increasing input rate, the FFLI output builds up a DC base and the *V* amplitude

gets higher eventually reaching Θ. This mode occurs if $\frac{V_{ff}}{\tau_{ff}} < \Theta_o$ is satisfied.

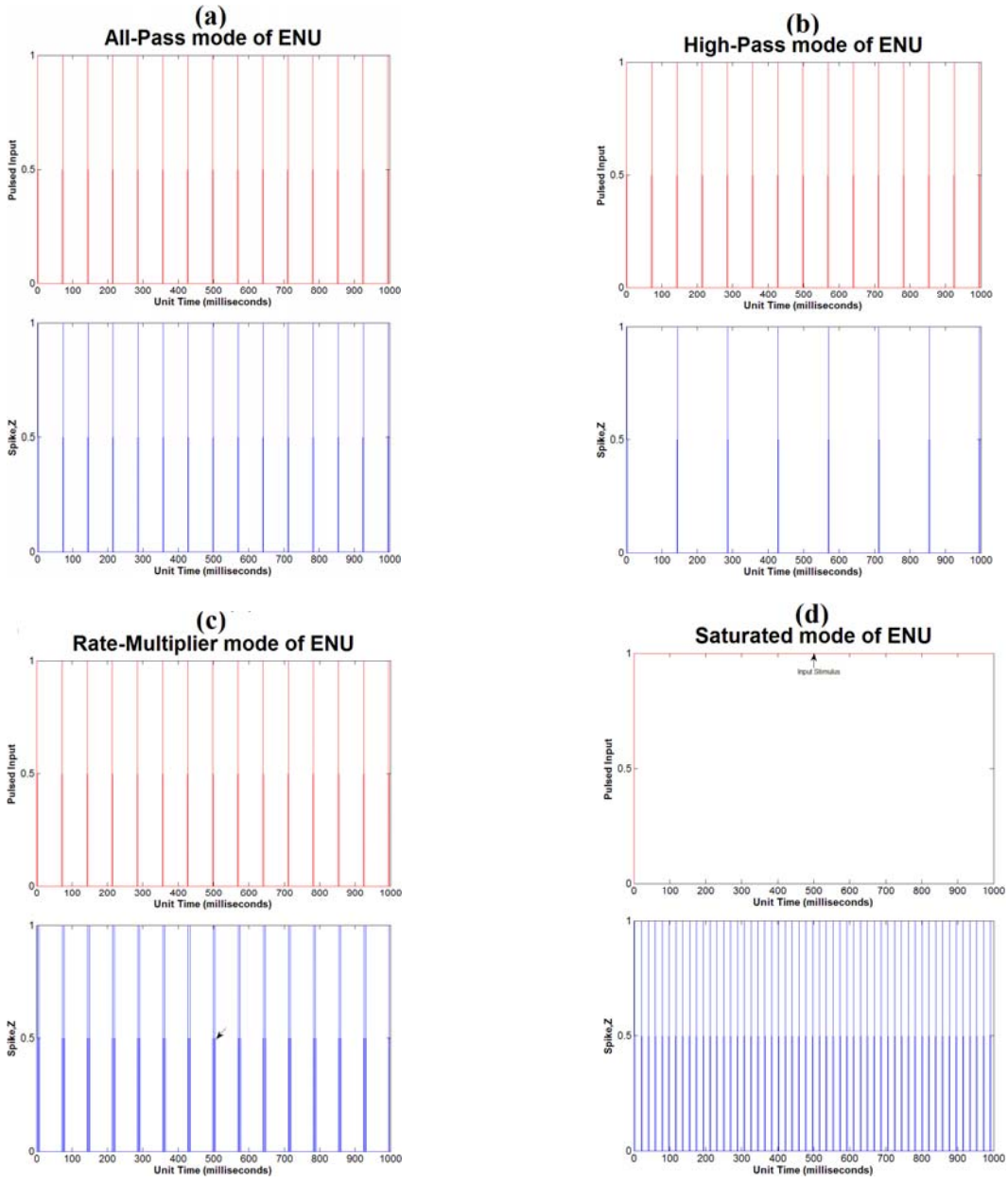

Figure 1.8. Different firing modes of an ENU. (a) All-pass mode: every input stimulus (red) results in ENU spiking (blue). (b) High-pass mode: ENU spiking occurs by skipping inputs (≥1, here just 1) between inputs that succeeded in causing spike. That is, it acts as a high-pass filter where inputs with low rates are filtered out. (c) Rate-multiplier mode: Single input stimulus causes more than one spike output (here 2, arrow). (d) Saturated mode: Input pulses with very short intervals produce a DC LI output and result in a maximum NMPG spiking rate decoupled from the input spiking rate.

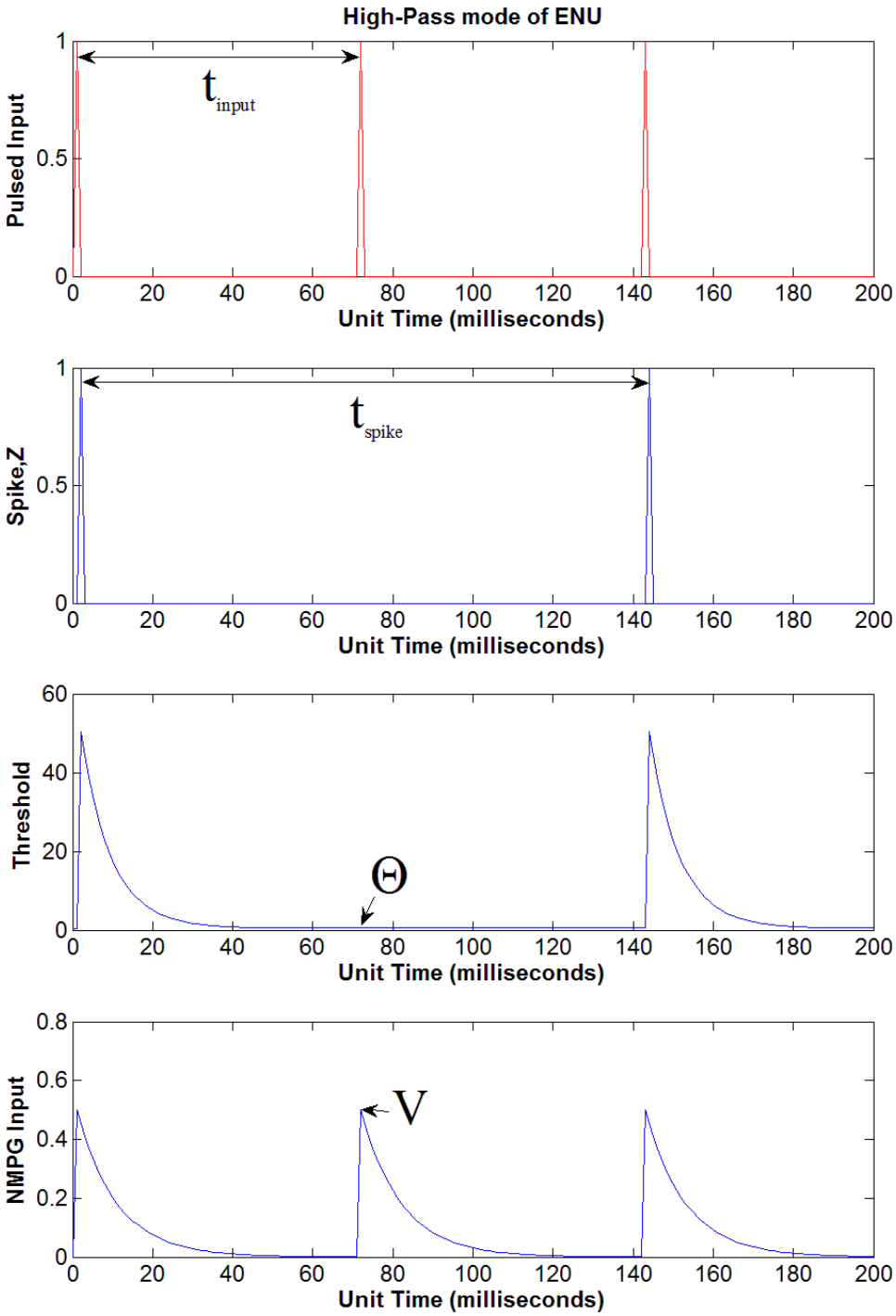

Figure 1.9. Snapshot of Figure 1.8b (High-Pass mode) demonstrating that the soma input (V, arrow of bottom plot) triggered by the second input (red, top plot) does not succeed in causing a spike because $V < \Theta$. Thus the inter-spike interval (t_{spike}) is wider than inter-input interval (t_{input}). That is, ENU at high-pass mode behaves like a high-pass filter as it filters out inputs with low rates.

Another mode the ENU can exhibit is the rate-multiplier mode (Fig. 1.8c). During this mode a single input can result in more than one spike (Fig. 1.8c arrow). This is because the soma input produced by the single input is strong enough that its decay still exceeds the threshold during the intra-spike interval (Fig. 1.10). Similar to all-pass firing mode, rate-multiplier modes can occur if $\frac{V_{ff}}{\tau_{ff}} \geq \Theta_o$ is satisfied. But in addition to this other conditions apply. That is, if $\tau_{ff} < \tau_{pg}$ and $V_{pg} > \frac{V_{ff}}{\tau_{ff}}$ then the ENU usually does not exhibit rate-multiplier mode. However this is not a sufficient condition because this mode may still be exhibited in at a later input impulse because, unlike soma threshold, the FFLI is not reset by soma firing. Rate-multiplier mode may also occur in cases when w_{ff} is adaptive and hence changing.

Finally, during saturated mode (Fig. 1.8d & 1.11) continuous spiking occurs within a particular total stimulus interval. The onset of this mode depends on the chosen parameters of the ENU. This mode occurs if the inter-input interval is very short, producing a large DC baseline. It results in soma threshold not able to reach its resting (Θ_o) level (Fig. 1.11). We shall call this Θ oscillation. This oscillation occurs around the plateau of the soma input (V) as shown in Figure 1.12a. The V plateau as the oscillatory baseline remains unchanged in cases with more than one ENU connected via the linking-field (Fig. 1.13a). In other words, Θ oscillates before V amplitude modulation (arrowhead, Fig. 1.13) by the linking field. The plateau level of V is determined by the FFLI output (Fig. 1.12b). Thus FFLI outputs can cause NMPG to oscillate.

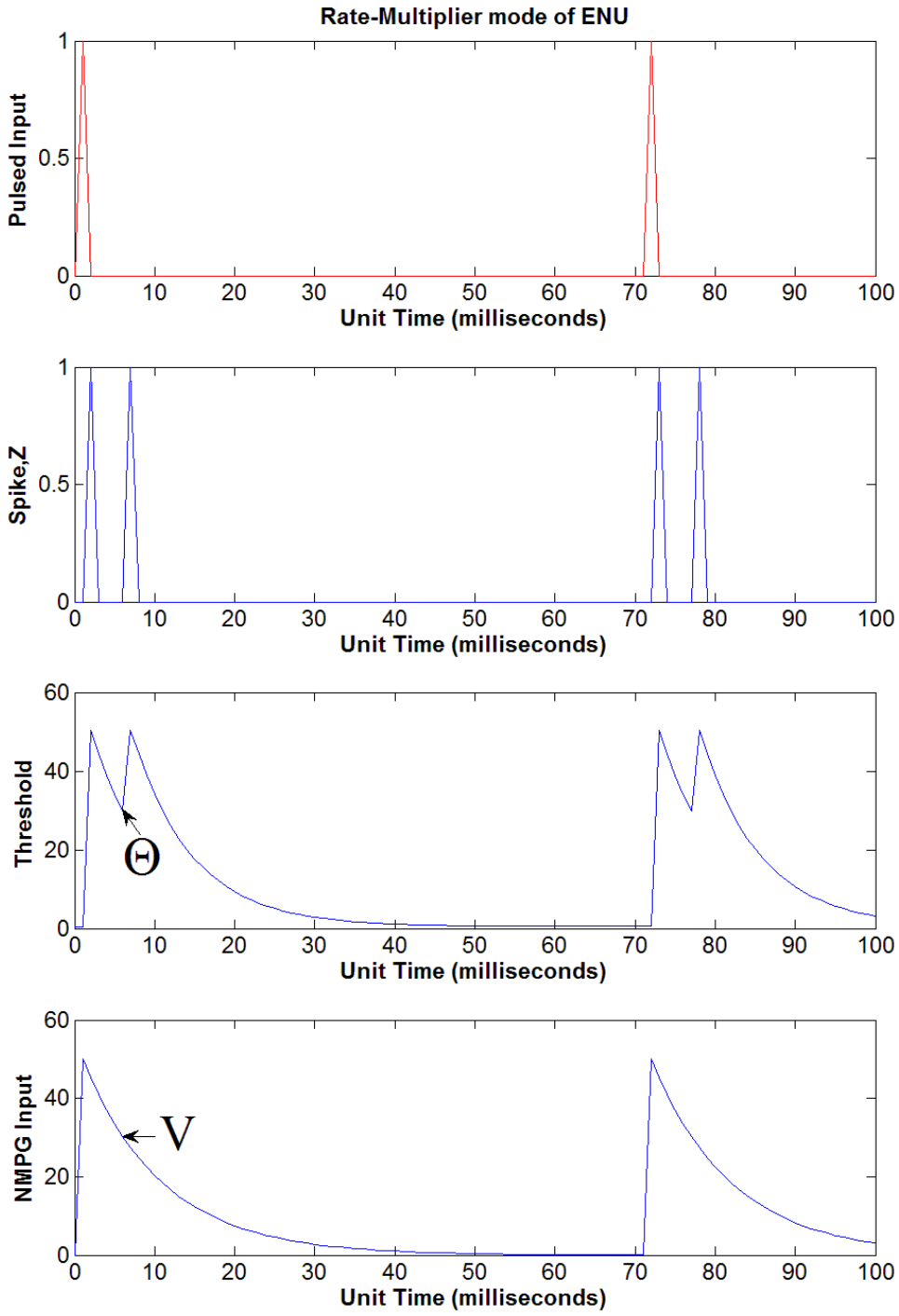

Figure 1.10. Snapshot of Figure 1.8c (Rate-Multiplier mode) demonstrating that the soma input (bottom plot) triggered by the input (red, top plot) succeeds ($V \geq \Theta$) in causing the first spike. Because of the success, the threshold is reset (to V_{pg}) and decays exponentially. Thus, $V < \Theta$. However at around 7ms magnitude of the decaying V (arrow of bottom plot) exceeds that of the decaying Θ (arrow of third plot). Thus, $V \geq \Theta$ results in a second spike caused by a single input. The second threshold reset and the already decaying soma input means that $V < \Theta$ at any given instant of time after the second spike.

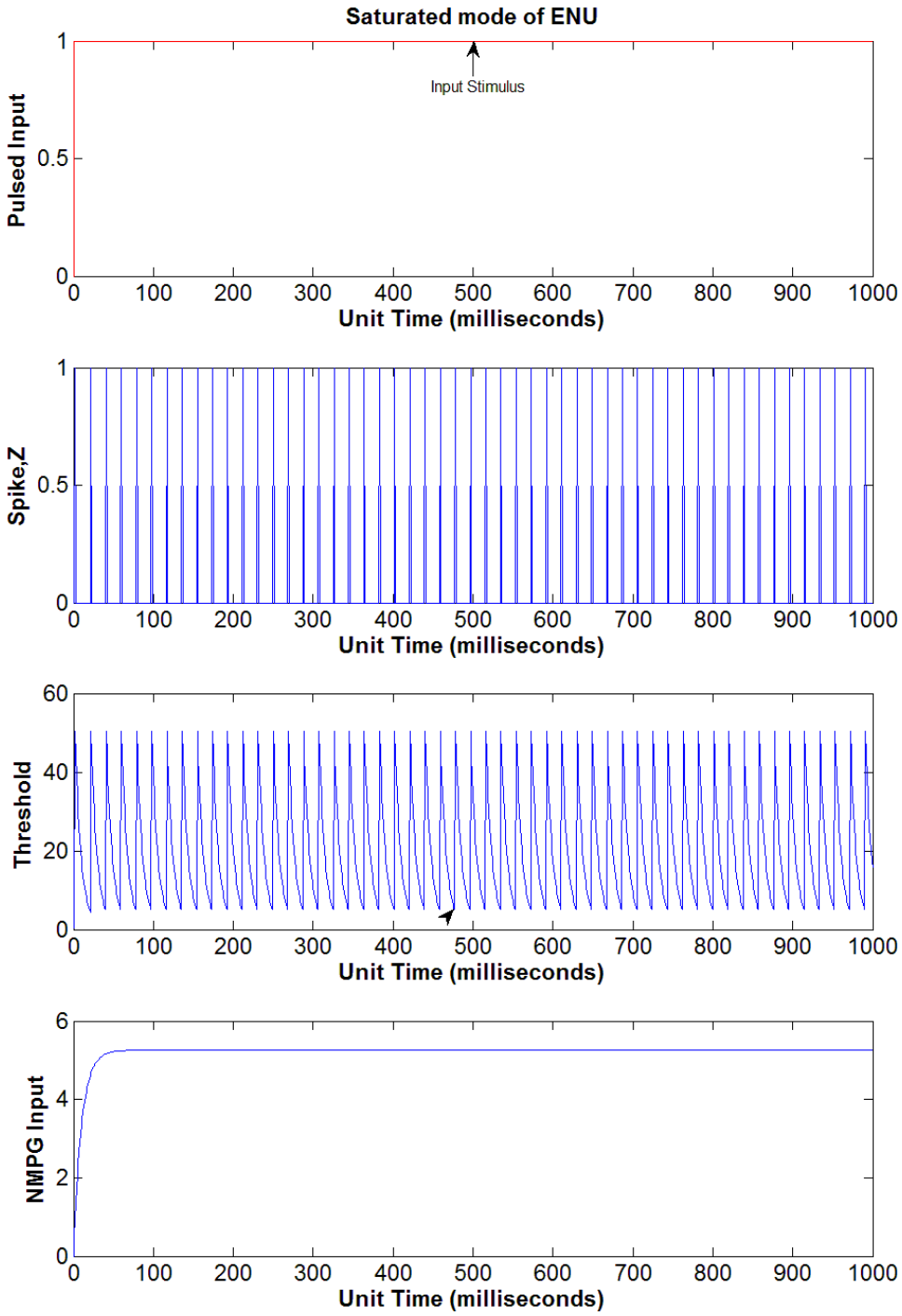

Figure 1.11. Snapshot of Figure 1.8d (Saturated mode) demonstrating that wide pulse inputs (top plot) cause the soma input (bottom plot) to have a DC-like feature. If this soma input satisfies the condition $V \geq \Theta$, then the soma threshold keeps oscillating (arrow head in third plot) above its resting (Θ_o) value. For a chosen set of parameters this means that the ENU produces a maximum number of spikes (second plot) during the total stimulus interval. In the case above, 53 spikes in 1 second of stimulus.

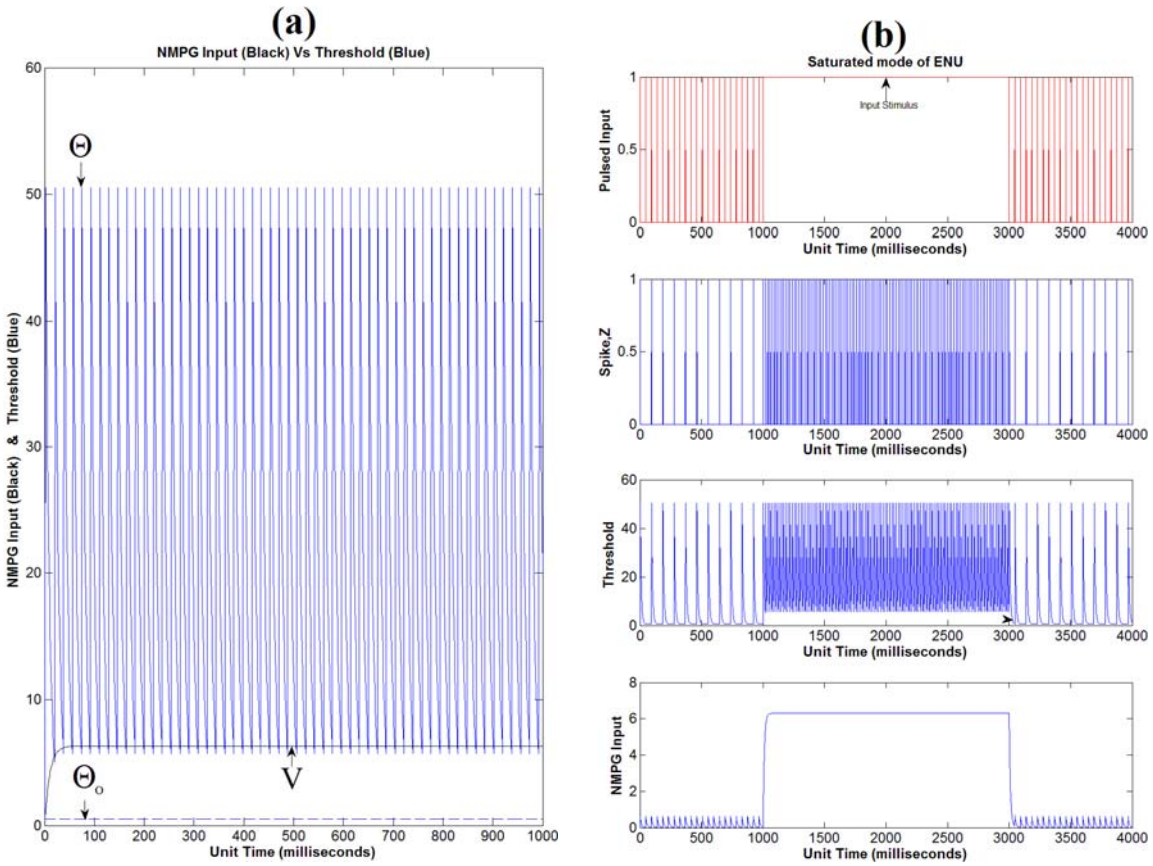

Figure 1.12. Plots for analysis of the saturated mode in a single ENU.

(a) Soma input and threshold (of Fig.1.11) in a single plot. This view demonstrates that the threshold (Θ) never reaches its resting value (Θ_o), rather Θ oscillates with its base as the V level.

(b) Plot for case when ENU receives standard input pulses (top) in the first and last seconds but a single pulsed input for the middle three seconds. During standard input pulses, the ENU is in high-pass mode but gets into saturated mode (second plot) as soon as the DC plateau is large enough (third plot). But as soon as the input reverts back to standard pulse the ENU goes back to high-pass mode. This is because the feeding field output and hence the soma input (bottom) decays back from the plateau. This means that the soma threshold (Θ) now has the opportunity to return to Θ_o (arrow, third plot). If the ENU instead receives impulsive volley inputs at inter-spike interval T, V will build up a DC plateau maximum equal to $\frac{1}{\mathrm{T}}\sum_{\forall j} w_{ff_j} \cdot F_j^{inputs}$. This figure mimics the effect of such a plateau. For biological ranges of T/τ, however, the plateau will be

$$\frac{\sum_{\forall j} w_{ff_j} \cdot F_j^{inputs}}{\mathrm{T}} \quad \frac{e^{-\mathrm{T}/\tau}}{1-e^{-\mathrm{T}/\tau}} \quad < \quad \frac{\sum_{\forall j} w_{ff_j} \cdot F_j^{inputs}}{\mathrm{T}} .$$

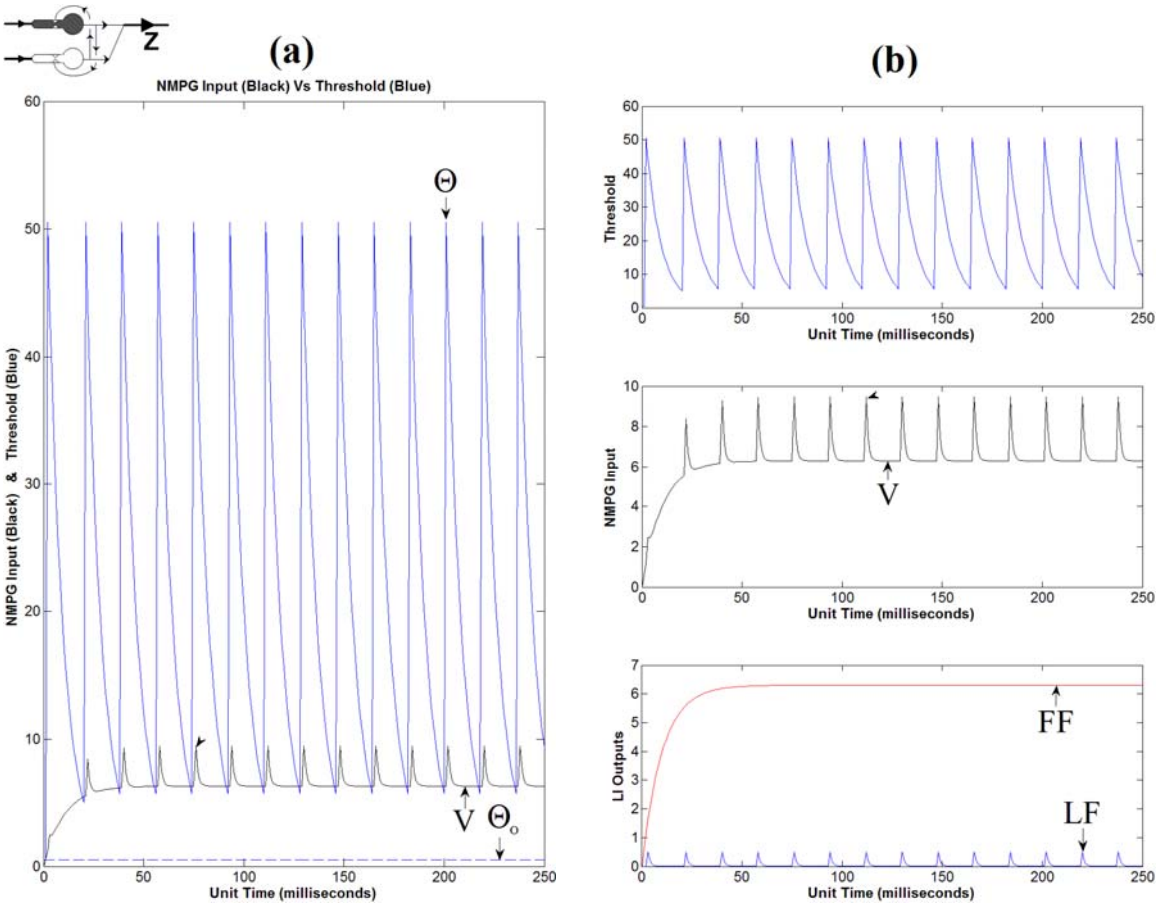

Figure 1.13. Plots for analysis of the saturated mode in a single ENU (shaded ENU, inset) when two ENU are connected via their linking fields.

(a) Soma input and threshold in a single plot. The soma input (V) unlike Figure 1.12a has a saw-tooth like feature (arrowhead). However the threshold (Θ) still never reaches its resting value (Θ_o) and oscillates around the base of the V saw-tooth.

(b) Plot shows the source of V seen in (a). The bottom figure shows that the saw-tooth feature of V (middle) is caused by the outputs (LF) from linking-field leaky-integrator (LFLI) and the plateau of V by the outputs (FF) from feeding-field leaky-integrator (FFLI).

With all these possible firing modes and the nonlinear behavior of the ENU one can see how this demonstrates the versatility of the ENU as a population neuron model. For instance, all-pass mode only ENU would be disadvantageous over other models, say I&F model due to the relatively complicated equations governing all-pass mode of an ENU

[Wells 2010, Ch.9]. However, high-pass mode ENU's in a network produce a phenomenon where the ENU spiking from each successive layer decreases resulting in an evanescent wave-like packet (Fig. 1.14). This phenomenon is consistent with brain signal processi-ng and hence can be implemented to test Malsburg's "binding" theory [Malsburg 1999].

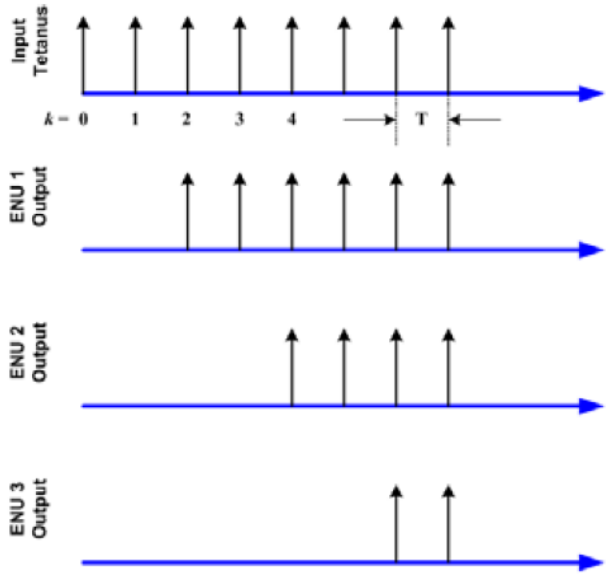

Figure 1.14. Illustration adopted from [Wells 2010, Ch.9] showing a simple ENU high-pass firing chain for a network consisting of three one-dimensional layers of neurons. The neural outputs from the end receiving stimulus to the third neural layer end demonstrate evanescent wave-like packets.

It was mentioned earlier that the terms "dendrite" and "soma" used for the ENU compartments do not correspond to those of biological neuron. There have been evidences to support the view that the ENU proxies for neuron pools [Wells et al. 2006]. Thus ENU outputs represent properties of a neuron pool or neuron population comprising hundreds to thousands of biological neurons. Freeman [Freeman 1972] defines "neuron population" as set of densely interconnected neurons with common input and same sign output. He further defines "aggregates" as neural mass with common input but zero

functional connection density even if anatomical connections exist within it.

In conclusion, the ENU differs from the integrate and fire (I&F) model [Burkitt 2006a, 2006b], another proxy neuron population model, primarily because the ENU incorporates refractory mechanisms and a variable threshold. However with respect to these general properties of the ENU, there are other model neurons/neuromimes [MacGregor & Lewis 1977]. What differentiates the ENU from these other models is the presence of linking-field part of the dendrite component modulating the feeding-field output.

Current APCNN's are designed for engineering applications, particularly image processing and hence these networks depart from biological plausibility. For instance, the PCNN's designed with ENUs produce wave-like firing action across the network (called auto-waves) via its linking-field connections, with each network representing a pixel [Johnson & Ritter 1993, Johnson 1994]. These networks are usually not connected with each other. Even some PCNNs that claim to be physiologically motivated [Broussard 1997] implement mathematical functions and techniques that diverge from biological plausibility. That is, it employs techniques or short-cuts to decrease the amount of computation for real-world engineering application. These arguments, in addition to the SR approach using model-reference principle employed here, let us to believe that the APCNN developed in this thesis is closer to biology than the current APCNNs.